Abstract. This supplement provides mesh-construction details, product-availability notes, sensitivity diagnostics, uncertainty summaries, and the numerical tables and figures supporting the main manuscript.

Abbreviations used in this supplement

UC – upwelling cell, as defined and enumerated in Methods §2.1 of the main manuscript (the five Benguela UCs: Cape Frio, Walvis Bay, Lüderitz, Cape Columbine, and Cape Peninsula). **BUS** – Benguela Upwelling System; **nBUS / sBUS** – northern / southern Benguela. **SST** – sea-surface temperature. **L4** – Level-4 (gap-filled, gridded) satellite SST analysis. **GHRSST** – Group for High Resolution Sea Surface Temperature. **OSTIA** – Operational Sea Surface Temperature and Ice Analysis (ca. 0.05° L4 SST). **OSPO** – the National Oceanic and Atmospheric Administration (NOAA) Office of Satellite and Product Operations Geo-Polar Blended analysis (ca. 0.05° L4 SST). **AVHRR_OI** – Advanced Very High Resolution Radiometer Optimum Interpolation (ca. 0.25° L4 SST). **MW_OI** – Microwave Optimum Interpolation (ca. 0.25° L4 SST). **NESDIS** – National Environmental Satellite, Data, and Information Service. **ETOPO** – NOAA Earth Topography global relief model. **NUD**, **NUE**, **TCU** – number of upwelling days, number of upwelling events, and total cumulative upwelling magnitude (the phenology metrics defined in main-manuscript Methods §2.5). UI_{BR}, $UI_{\mathrm{SST}}^{(d_0)}$ – the segmented-breakpoint and fixed-distance upwelling indices defined in main-manuscript Methods §2.4 and §2.6. **AIC** – Akaike information criterion; **AICc** – small-sample corrected Akaike information criterion; **BIC** – Bayesian information criterion. **AR(1)** – first-order autoregressive residual model (coefficient ϕ); n_{eff} – effective (independent) sample size. **OLS** – ordinary least squares. **CI** – confidence interval; **IQR** – interquartile range; **CDF** – cumulative distribution function. **BH** – Benjamini–Hochberg false-discovery-rate adjustment. **MCC** – Matthews correlation coefficient; **BalAcc** – balanced accuracy; **KDE** – kernel density estimate. **ANN** – annual aggregate; **DJF / MAM / JJA / SON** – austral summer (December–February) / autumn (March–May) / winter (June–August) / spring (September–November).

Contents of this file

11. Table S8. AR(1)-corrected per-(UC, product, season) Pearson r between $\bar{D}_{\mathrm{in}}$ and $UI_{\mathrm{SST}}^{(d_0)}$ at each d_0, with BH-adjusted seasonal q values for r_{50}.

12. Table S9. Block-bootstrap 95 % intervals on the main statistics, namely the Lüderitz r_{50}, the sBUS SST-structure-only fraction, and the median x_b per UC, with block sizes of 25 km and 50 km reported separately.

13. Table S10. AR(1)-corrected per-(UC, product) phenology summary: across-year median and range of $\mathrm{NUD}_{\mathrm{BR}}$, $\mathrm{NUE}_{\mathrm{BR}}$, $\mathrm{TCU}_{\mathrm{BR}}$.

14. Figure S1. Daily detection and annual upwelling-day phenology, matching Figure 5 of manuscript version 3.

15. Figure S2. Per-UC daily p_{active} time series 2015–2025 across four products.

16. Figure S3. Cohen's κ against wind marginal probability per (UC, product), with the saturation regime marked.

17. Figure S4. Per-UC empirical CDFs of per-profile 95 % bootstrap CI widths on $\hat{x}_b$, computed on a stratified random sample of 4000 accepted 2020 profiles.

18. Figure S5. Full-size representative accepted and rejected OSTIA breakpoint-regression profiles stratified by season.

Introduction

This document provides per-product index-quantity availability, coverage-artefact documentation for two AVHRR product-UC pairs, reproducibility details, the AR(1)-corrected per-(UC, product, season) numerical detail behind the figures and summary tables of the main manuscript, and the supporting tables for the model-evidence comparison (AIC / AICc / BIC, n_{eff}), the six-dimensional sensitivity grid, the paired-classifier statistics block, the block-bootstrap intervals on the principal statistics, and the per-profile $\hat{x}_b$ bootstrap identifiability diagnostic on a stratified population sample.

Text S1. UC selection, mesh construction, inputs, and reproducibility

UC selection

Lutjeharms and Meeuwis (1987) delineated eight wind-driven UCs from three years of weekly multichannel SST imagery, namely Cunene, Namibia, Walvis Bay, Lüderitz, Namaqua, Columbine, Peninsula, and Agulhas (transitional). Kämpf and Chapman (2016) list six in their Figure 7.2, including a Namaqualand UC at ca. 28.5° S. Hutchings et al. (2009) discuss upwelling at Cape Frio, Walvis Bay, Lüderitz, Cape Columbine / St Helena Bay, and Cape Point without enumerating a named set. The five UCs used in the main manuscript are the five at which the breakpoint regression accepts profiles unambiguously and persistently across all four SST products; the Namaqualand UC of Kämpf and Chapman (2016) sits in the Lüderitz–Cape Columbine transition zone and is treated as part of the southernmost nBUS in this analysis. The five UC windows (defined in Methods §2.1 of the main manuscript) contain 189 unique mesh transects: 50 at Cape Frio, 49 at Walvis Bay, 49 at Lüderitz, 18 at Cape Columbine, and 23 at Cape Peninsula. The Cape Columbine and Cape Peninsula counts are smaller because those two windows are truncated at their inter-UC midpoint (Methods §2.1) rather than because the UCs are physically narrower.

Mesh construction

The mesh is generated by tracing streamlines of a discrete Laplace potential field ϕ over the ocean domain bounded by the smoothed Benguela coast and a 500 km coast-distance outer contour. Bathymetric inputs are taken from the 1-arc-minute NOAA ETOPO record retrieved through the `marmap` R interface; the coastline is projected to a local azimuthal-equidistant frame centred on the coast mean and resampled as a 1 km smoothed spline. Two bay-bridge polylines are overlaid, one across the mouth of St Helena Bay near 32.8° S and one across the mouth of False Bay near 34.4° S; the bridges replace the inside-bay portions of the coastline with a short offshore path so that coastal seeds at the bay mouths project transects into the open ocean

rather than into the bay interior. The outer boundary is constructed by rasterising nearest-coast Euclidean distance on a 5 km grid, masking land, and extracting the 500 km isoline. The discrete Laplace equation $\nabla^2\phi = 0$ is solved on the same 5 km grid with Dirichlet conditions $\phi = 0$ on a ca. 3 km coast band and $\phi = 1$ on a matching band along the outer contour; the five-point stencil sparse linear system is assembled in `scipy.sparse` and solved with `spsolve`. Coastal seeds are placed at ca. 7 km along-coast spacing on the smoothed coast curve, with tighter spacing along the bay-bridge segments where coast orientation changes over a short distance. From each seed a streamline is traced in 2.5 km steps along $\nabla\phi/|\nabla\phi|$, terminating at the 500 km outer contour. Five pruning passes are applied in sequence to the raw streamline set: (i) iterative removal of one member of every adjacent-crossing pair until no adjacent crossings remain; (ii) thinning of crowded outer endpoints south of 34° S, where streamlines converge on a narrow offshore arc; (iii) enforcement of $\geq$18 km outer and $\geq$24 km coast spacing in the False Bay sector, which otherwise carries a cluster generated by the False Bay bridge; (iv) enforcement of $\geq$10 km outer and $\geq$8 km coast spacing in the Table Bay head sector; and (v) removal of any streamline shorter than 90 % of the 500 km outer distance, which identifies streamlines that terminated prematurely in re-entrant bay geometry. A final crossing-removal pass catches any adjacencies newly exposed by the four intermediate passes. The retained mesh contains 742 transects, each sampled at 480 sigma nodes at uniform fractions of arc length along its streamline.

Mesh and arc-length to coast-distance reparameterisation

The cross-shore mesh covers the bounding box 5° E to 22.5° E by 12° S to 40° S. The 189 transects used in the present analysis are the subset that falls inside the five UC windows defined above; the remaining 564 transects, covering the Benguela coast outside those five windows, were excluded by UC-window definition only, with no further data-quality filter applied to narrow the population. The transects are gradient lines (streamlines) of a Laplace potential ϕ, with $\phi = 0$ on the coast and $\phi = 1$ on the outer contour. The Laplace operator is not eikonal, so $|\nabla\phi|$ varies in space and the per-transect streamline arc-length ℓ (column `line_length_km` in the persisted parquet) varies between transects: in straight-coast regions $\ell \approx 500$ km, but on streamlines originating in the bays flanking Cape Columbine ℓ reaches ca. 540–600 km. The cross-shore regression coordinate in the breakpoint regression (manuscript Methods §2.2) is $x = \sigma \cdot \ell$ (arc-length), and the offshore-segment acceptance criterion is therefore in arc-length, $\ell - x_b \geq 100$ km on each transect. Reported x_b and d_0 values throughout the main manuscript and the supplementary tables are converted to coast-distance via the linear streamline-stretch approximation $x_{\mathrm{coast}} = x \cdot 500/\ell$. The approximation is exact for straight-coast transects and a sub-10 % deviation elsewhere except at Cape Columbine, where the stretch factor reaches 1.10–1.20.

Inputs

The four SST products are GHRSST Level-4 analyses at native resolution: OSTIA at ca. 0.05° (Donlon et al., 2012; Good et al., 2020; Worsfold et al., 2024); the NOAA/NESDIS Geo-Polar Blended OSPO at ca. 0.05° (Maturi et al., 2017); AVHRR_OI at ca. 0.25° (Reynolds et al., 2007; Banzon et al., 2016); and MW_OI at ca. 0.25° (Wentz et al., 2000; Chelton and Wentz, 2005). OSTIA, OSPO, and MW_OI cover the full 2015-01-01 to 2025-12-31 window (eleven Lamont years 2015–2025); AVHRR coverage starts in 2016 and provides ten complete Lamont years (2016–2025), consistent with the per-UC phenology row counts in Table S10. ERA5 hourly 10-m winds at the native 0.25° grid for the same window (Hersbach et al., 2020) support the wind-based comparison. The per-(product, day, transect) breakpoint quantities $\{\beta_{\mathrm{in}}, \beta_{\mathrm{off}}, x_b, \widehat{T}_{\mathrm{bg}}\}$ are read from the breakpoint-output tables described in Methods §2.2 of the main manuscript.

Reproducibility

The processing scripts of the present analysis are publicly available at https://github.com/ajsmit/ucxd in the `uidx/paperA` sub-project, together with the UC-window definitions table, the per-(product, day, transect) UI_{BR} outputs, the AR(1)-corrected derived tables that feed every main-text result, and the figure and table rendering scripts. The per-UC membership file uidx/paperA/audit/paperA_cell_transects.csv records the 189 transects used in the five UC windows.

Text S2. Per-product index-quantity availability

The three components of UI_{BR} have asymmetric availability across the four products in the UC windows. The breakpoint quantities β_{in} and x_b are computable wherever the breakpoint regression is accepted; the inshore SST drawdown $\bar{D}_{\mathrm{in}}$ additionally requires the SST profile to be valid from $x = 0$ to $x = x_b$. Under the AR(1)-corrected acceptance criterion used for the main results, OSTIA and OSPO retain accepted-profile populations in every UC, whereas AVHRR and MW_OI return zero accepted profiles in the tested UC-season combinations (Table S1). The main climatology, fixed-distance comparison, phenology, paired classifier, and block-bootstrap intervals therefore use OSTIA and OSPO only. The baseline four-product availability remains useful for product-resolution diagnosis: MW_OI has a structural ca. 100 km microwave coastal mask, and AVHRR has sparse usable inshore SST at Cape Frio and Cape Peninsula. The AR(1)-corrected seasonal medians are tabulated in Table S7.

Text S3. Coverage-artefact handling

Under the AR(1)-corrected analysis, AVHRR and MW_OI do not contribute to the main paired-classifier results because the corrected acceptance set returns no accepted coarse-product profiles in the tested UC-season combinations (Table S1).

Table S1: Per-(UC, product, season) AR(1) residual decorrelation coefficient ϕ, implied median effective sample $n^{\star}_{\mathrm{eff}}$, and resulting change in the per-UC daily activity fraction p_{active} when the AIC bar is recomputed with $n^{\star}_{\mathrm{eff}}$ in place of the unique-pixel count. Negative $\Delta p_{\mathrm{active}}$ values indicate acceptance loss under the AR(1)-corrected criterion. AVHRR and MW_OI rows are omitted: at the ca. 0.25° native resolution of these products, the unique-pixel count per profile is too small ($n_{\mathrm{baseline}} \leq 23$) for $n^{\star}_{\mathrm{eff}}$ to clear the AIC bar, and the AR(1)-corrected $p^{n_{\mathrm{eff}}}_{\mathrm{active}}$ is zero at every (UC, season). OSTIA and OSPO retain accepted-profile populations and form the main-result set used in the manuscript.

UC	Prod.	Season	n_{baseline}	ϕ	$n^{\star}_{\mathrm{eff}}$	$p^{\mathrm{base}}_{\mathrm{active}}$	$p^{n_{\mathrm{eff}}}_{\mathrm{active}}$	$\Delta p_{\mathrm{active}}$
Cape Frio	OSTIA	DJF	92.0	0.909	4.37	0.989	0.860	-0.129
Cape Frio	OSTIA	MAM	92.0	0.910	4.33	0.938	0.668	-0.270
Cape Frio	OSTIA	JJA	92.0	0.918	3.91	0.906	0.394	-0.512
Cape Frio	OSTIA	SON	92.0	0.928	3.43	0.951	0.444	-0.506
Cape Frio	OSPO	DJF	92.0	0.909	4.37	0.989	0.890	-0.100
Cape Frio	OSPO	MAM	92.0	0.910	4.33	0.946	0.694	-0.252
Cape Frio	OSPO	JJA	92.0	0.918	3.91	0.899	0.415	-0.484
Cape Frio	OSPO	SON	92.0	0.928	3.43	0.953	0.472	-0.482
Walvis Bay	OSTIA	DJF	93.0	0.917	4.04	0.819	0.488	-0.331
Walvis Bay	OSTIA	MAM	93.0	0.943	2.73	0.682	0.137	-0.545
Walvis Bay	OSTIA	JJA	93.0	0.950	2.41	0.681	0.039	-0.642
Walvis Bay	OSTIA	SON	93.0	0.894	5.22	0.886	0.727	-0.159
Walvis Bay	OSPO	DJF	93.0	0.917	4.04	0.807	0.484	-0.324
Walvis Bay	OSPO	MAM	93.0	0.943	2.73	0.673	0.142	-0.530
Walvis Bay	OSPO	JJA	93.0	0.950	2.41	0.683	0.052	-0.630
Walvis Bay	OSPO	SON	93.0	0.894	5.22	0.883	0.734	-0.149
Lüderitz	OSTIA	DJF	91.0	0.884	5.61	0.999	0.992	-0.006
Lüderitz	OSTIA	MAM	91.0	0.910	4.28	0.991	0.890	-0.101
Lüderitz	OSTIA	JJA	91.0	0.922	3.71	0.995	0.747	-0.248
Lüderitz	OSTIA	SON	91.0	0.903	4.62	0.999	0.957	-0.041
Lüderitz	OSPO	DJF	91.0	0.884	5.61	0.999	0.992	-0.007
Lüderitz	OSPO	MAM	91.0	0.910	4.28	0.987	0.895	-0.092
Lüderitz	OSPO	JJA	91.0	0.922	3.71	0.996	0.783	-0.213
Lüderitz	OSPO	SON	91.0	0.903	4.62	1.000	0.960	-0.040
Cape Columbine	OSTIA	DJF	101.0	0.897	5.47	1.000	0.963	-0.037
Cape Columbine	OSTIA	MAM	101.0	0.916	4.42	1.000	0.918	-0.082
Cape Columbine	OSTIA	JJA	101.0	0.923	4.05	0.945	0.644	-0.302
Cape Columbine	OSTIA	SON	101.0	0.905	5.04	0.975	0.861	-0.113
Cape Columbine	OSPO	DJF	101.0	0.897	5.47	0.998	0.968	-0.030
Cape Columbine	OSPO	MAM	101.0	0.916	4.42	1.000	0.930	-0.069
Cape Columbine	OSPO	JJA	101.0	0.923	4.05	0.953	0.696	-0.257
Cape Columbine	OSPO	SON	101.0	0.905	5.04	0.973	0.874	-0.099
Cape Peninsula	OSTIA	DJF	93.0	0.902	4.80	0.911	0.779	-0.131
Cape Peninsula	OSTIA	MAM	93.0	0.915	4.11	0.931	0.710	-0.220
Cape Peninsula	OSTIA	JJA	93.0	0.920	3.87	0.738	0.244	-0.493
Cape Peninsula	OSTIA	SON	93.0	0.915	4.11	0.817	0.439	-0.378
Cape Peninsula	OSPO	DJF	95.0	0.902	4.90	0.931	0.829	-0.102
Cape Peninsula	OSPO	MAM	95.0	0.915	4.20	0.955	0.778	-0.177
Cape Peninsula	OSPO	JJA	95.0	0.920	3.95	0.772	0.301	-0.470
Cape Peninsula	OSPO	SON	95.0	0.915	4.20	0.825	0.503	-0.321

Table S2. Acceptance-threshold sensitivity-grid results, pre-AR(1) assay. Per criterion: baseline, tested values, the Lüderitz annual r_{50} on OSTIA (range across tested values), the OSTIA p_{active} range across (UC, criterion-value) tuples, and the Walvis Bay-specific OSTIA p_{active} range (the most acceptance-sensitive UC). The Lüderitz r_{50} remains negative at every tested value on every criterion; all five OSTIA UCs satisfy $P(x_b > 50\,\mathrm{km}) \geq 0.5$ at every tested value on every criterion. The AR(1)-corrected main results in the present paper are reported in Tables S1, S5, and S7–S10.

Criterion	Baseline	Tested values	Lüderitz r_{50}	OSTIA p_{active}	Walvis Bay p_{active}
ΔAIC bar	4.0	2, 4, 6, 8	-0.159 to -0.159	0.74–0.92	0.74–0.74
slope ratio	2.0	1.5, 2, 2.5, 3	-0.159 to -0.157	0.58–0.93	0.58–0.80
min offshore (km)	100.0	50, 100, 150, 200	-0.159 to -0.141	0.50–0.92	0.50–0.74
edge buffer (km)	10.0	10, 25, 50, 75	-0.163 to -0.159	0.67–0.92	0.72–0.74
pixel rule	across_thinned	across_thinned, native	-0.164 to -0.159	0.74–1.00	0.74–0.77
p_{active} threshold	0.5	0.3, 0.5, 0.7	-0.159 to -0.159	0.74–0.92	0.74–0.74

Table S3. AIC, AICc, and BIC side-by-side comparison on the Cape Columbine DJF 2020 test subset across all four SST products. X-only and Y-only columns count profiles accepted by the first and second rule in each rule pair, respectively.

Rule pair	Product	Both reject	X-only	Y-only	Both accept	Agreement (%)
AIC vs AICc	OSTIA	0	0	0	1,638	100.0
AIC vs AICc	OSPO	0	0	0	1,638	100.0
AIC vs AICc	AVHRR	7	4	0	819	99.5
AIC vs AICc	MW_OI	3	8	0	1,551	99.5
AIC vs BIC	OSTIA	0	0	0	1,638	100.0
AIC vs BIC	OSPO	0	0	0	1,638	100.0
AIC vs BIC	AVHRR	7	4	0	819	99.5
AIC vs BIC	MW_OI	3	8	0	1,551	99.5
AICc vs BIC	OSTIA	0	0	0	1,638	100.0
AICc vs BIC	OSPO	0	0	0	1,638	100.0
AICc vs BIC	AVHRR	11	0	0	819	100.0
AICc vs BIC	MW_OI	11	0	0	1,551	100.0

Table S4. Self-contained p_{active} threshold sensitivity for the SST-based annual upwelling-day count on the two fine-resolution products. Values are across-year medians of $\mathrm{NUD}_{\mathrm{BR}}$ (days per Lamont year) after reclassifying the archived daily UC-window activity fractions at $p_{\mathrm{active}} \geq 0.3$, 0.5, and 0.7, using the same single-quiet-day bridge and complete-year filter ($n_{\mathrm{days}} \geq 330$) as Stage 4c. The 0.5 column reproduces the operational phenology parquet exactly.

UC	Product	n	$p_{\mathrm{active}} \geq 0.3$	$p_{\mathrm{active}} \geq 0.5$	$p_{\mathrm{active}} \geq 0.7$
Cape Frio	OSTIA	10	359.0	353.0	336.5
Cape Frio	OSPO	10	351.5	349.0	330.5
Walvis Bay	OSTIA	10	311.0	278.0	238.5
Walvis Bay	OSPO	10	316.0	274.0	227.0
Lüderitz	OSTIA	10	365.0	365.0	363.5
Lüderitz	OSPO	10	359.0	359.0	356.5
Cape Columbine	OSTIA	10	365.0	363.0	360.0
Cape Columbine	OSPO	10	356.0	353.0	348.5
Cape Peninsula	OSTIA	10	359.5	347.5	289.0
Cape Peninsula	OSPO	10	353.0	347.5	293.0

Table S5: AR(1)-corrected paired-classifier diagnostic between the SST-structure detector ($p_{\mathrm{active}} \geq 0.5$) and the Bakun-positive offshore-Ekman-transport wind detector. p_{SST} and p_{wind} are active-day prevalences; BalAcc is balanced accuracy; MCC is Matthews correlation coefficient; p_o is raw agreement; κ is Cohen's kappa. The four right-hand columns give the descriptive regime fractions.

UC	Product	Season	n	p_{SST}	p_{wind}	BalAcc	Sens.	Spec.	MCC	κ	active	quiet	SST-only	wind-only
Cape Frio	OSTIA	DJF	962	0.93	0.98	0.59	0.94	0.25	+0.10	+0.08	0.92	0.00	0.01	0.06
Cape Frio	OSTIA	MAM	1005	0.72	0.99	0.49	0.72	0.25	-0.01	-0.00	0.72	0.00	0.01	0.27
Cape Frio	OSTIA	JJA	1003	0.36	0.94	0.50	0.36	0.64	-0.00	-0.00	0.33	0.04	0.02	0.60
Cape Frio	OSTIA	SON	995	0.46	0.97	0.57	0.47	0.68	+0.05	+0.01	0.45	0.02	0.01	0.52

UC	Product	Season	n	p_{SST}	p_{wind}	BalAcc	Sens.	Spec.	MCC	κ	active	quiet	SST-only	wind-only
Cape Frio	OSPO	DJF	926	0.95	0.98	0.47	0.95	0.00	-0.03	-0.03	0.93	0.00	0.02	0.05
Cape Frio	OSPO	MAM	1000	0.76	0.99	0.44	0.76	0.12	-0.02	-0.01	0.75	0.00	0.01	0.24
Cape Frio	OSPO	JJA	984	0.39	0.93	0.53	0.40	0.66	+0.03	+0.01	0.37	0.04	0.02	0.56
Cape Frio	OSPO	SON	961	0.51	0.97	0.50	0.51	0.50	+0.00	+0.00	0.49	0.01	0.01	0.48
Walvis Bay	OSTIA	DJF	962	0.52	0.85	0.60	0.55	0.64	+0.14	+0.10	0.47	0.10	0.05	0.38
Walvis Bay	OSTIA	MAM	1005	0.12	0.94	0.53	0.12	0.93	+0.04	+0.01	0.11	0.06	0.00	0.83
Walvis Bay	OSTIA	JJA	1003	0.01	0.84	0.51	0.02	0.99	+0.03	+0.00	0.01	0.16	0.00	0.83
Walvis Bay	OSTIA	SON	995	0.76	0.83	0.52	0.76	0.27	+0.03	+0.03	0.63	0.05	0.13	0.20
Walvis Bay	OSPO	DJF	926	0.47	0.85	0.62	0.51	0.74	+0.18	+0.12	0.43	0.11	0.04	0.42
Walvis Bay	OSPO	MAM	1000	0.11	0.94	0.51	0.11	0.92	+0.02	+0.00	0.11	0.05	0.01	0.83
Walvis Bay	OSPO	JJA	984	0.04	0.85	0.51	0.04	0.99	+0.05	+0.01	0.03	0.15	0.00	0.81
Walvis Bay	OSPO	SON	961	0.77	0.83	0.52	0.78	0.27	+0.04	+0.04	0.65	0.05	0.13	0.18
Lüderitz	OSTIA	DJF	962	1.00	0.94	0.51	1.00	0.02	+0.13	+0.03	0.94	0.00	0.06	0.00
Lüderitz	OSTIA	MAM	1005	0.93	0.90	0.50	0.93	0.07	+0.00	+0.00	0.84	0.01	0.09	0.06
Lüderitz	OSTIA	JJA	1003	0.82	0.76	0.53	0.84	0.23	+0.07	+0.07	0.64	0.05	0.18	0.12
Lüderitz	OSTIA	SON	995	0.99	0.89	0.50	0.99	0.01	+0.01	+0.00	0.89	0.00	0.10	0.01
Lüderitz	OSPO	DJF	926	1.00	0.94	0.50	1.00	0.00	-0.01	-0.00	0.94	0.00	0.06	0.00
Lüderitz	OSPO	MAM	1000	0.93	0.90	0.51	0.93	0.09	+0.02	+0.02	0.83	0.01	0.09	0.07
Lüderitz	OSPO	JJA	984	0.85	0.77	0.50	0.85	0.16	+0.01	+0.01	0.65	0.04	0.20	0.12
Lüderitz	OSPO	SON	961	0.99	0.89	0.50	0.99	0.01	-0.00	-0.00	0.88	0.00	0.11	0.01
Cape Columbine	OSTIA	DJF	962	0.96	0.86	0.52	0.96	0.07	+0.06	+0.05	0.83	0.01	0.13	0.03
Cape Columbine	OSTIA	MAM	1005	0.93	0.75	0.51	0.93	0.08	+0.02	+0.02	0.70	0.02	0.23	0.05
Cape Columbine	OSTIA	JJA	1003	0.78	0.54	0.48	0.76	0.19	-0.05	-0.05	0.41	0.09	0.37	0.13
Cape Columbine	OSTIA	SON	995	0.94	0.78	0.51	0.94	0.08	+0.03	+0.02	0.73	0.02	0.20	0.05
Cape Columbine	OSPO	DJF	926	0.97	0.86	0.51	0.97	0.05	+0.02	+0.02	0.83	0.01	0.14	0.03
Cape Columbine	OSPO	MAM	1000	0.93	0.75	0.49	0.93	0.06	-0.02	-0.02	0.69	0.01	0.24	0.05
Cape Columbine	OSPO	JJA	984	0.83	0.53	0.49	0.81	0.16	-0.04	-0.03	0.43	0.07	0.39	0.10
Cape Columbine	OSPO	SON	961	0.94	0.78	0.50	0.94	0.06	-0.00	-0.00	0.73	0.01	0.21	0.05
Cape Peninsula	OSTIA	DJF	962	0.92	0.84	0.51	0.92	0.09	+0.02	+0.02	0.78	0.01	0.14	0.07
Cape Peninsula	OSTIA	MAM	1005	0.83	0.68	0.52	0.84	0.19	+0.04	+0.03	0.57	0.06	0.26	0.11
Cape Peninsula	OSTIA	JJA	1003	0.27	0.45	0.50	0.27	0.73	+0.01	+0.01	0.12	0.40	0.15	0.33
Cape Peninsula	OSTIA	SON	995	0.53	0.73	0.58	0.57	0.58	+0.13	+0.12	0.42	0.15	0.11	0.32
Cape Peninsula	OSPO	DJF	926	0.98	0.84	0.51	0.98	0.05	+0.06	+0.04	0.83	0.01	0.15	0.02
Cape Peninsula	OSPO	MAM	1000	0.90	0.68	0.53	0.92	0.13	+0.09	+0.07	0.62	0.04	0.28	0.05
Cape Peninsula	OSPO	JJA	984	0.33	0.45	0.51	0.34	0.67	+0.01	+0.01	0.15	0.37	0.18	0.30
Cape Peninsula	OSPO	SON	961	0.62	0.73	0.54	0.64	0.45	+0.08	+0.08	0.47	0.12	0.15	0.26

Table S6: Per-profile bootstrap diagnostic of $\hat{x}_b$ identifiability, computed on a stratified random sample of accepted 2020 profiles (100 profiles per (UC, product, season), pooled across the four austral seasons). Per (UC, product): the median width of the per-profile 95 % bootstrap interval on $\hat{x}_b$, the 25th–75th percentile range of that width, the fraction of profiles with width below 50 and below 100 km, and the fraction flagged bimodal (Gaussian KDE peaks separated by more than 50 km). N is the per-(UC, product) sample size summed across seasons.

Cell	Product	N	Median CI (km)	IQR (km)	frac < 50	frac < 100	frac bimodal
Cape Frio	OSTIA	400	27.8	17.0–71.9	0.69	0.82	0.10
Cape Frio	OSPO	400	22.2	16.8–39.4	0.78	0.91	0.06
Walvis Bay	OSTIA	400	27.9	22.4–39.4	0.82	0.91	0.06
Walvis Bay	OSPO	400	23.0	21.5–33.1	0.88	0.95	0.01
Lüderitz	OSTIA	400	22.4	16.9–39.0	0.80	0.90	0.06
Lüderitz	OSPO	400	17.2	16.7–27.5	0.90	0.96	0.03
Cape Columbine	OSTIA	400	23.1	17.1–44.3	0.77	0.87	0.09
Cape Columbine	OSPO	400	22.2	16.6–33.3	0.86	0.94	0.04
Cape Peninsula	OSTIA	400	22.6	16.7–43.8	0.78	0.91	0.07
Cape Peninsula	OSPO	400	21.5	16.5–28.4	0.85	0.91	0.02

Table S7: AR(1)-corrected per-(UC, product, season) climatological medians of $\bar{D}_{\mathrm{in}}$, x_b, β_{in}, and fixed-distance contrasts. Only OSTIA and OSPO are listed because AVHRR and MW_OI fail the AR(1)-corrected acceptance criterion in these UC-season tests.

UC	Product	Season	n	$\bar{D}_{\mathrm{in}}$	x_b	β_{in}	UI_{50}	UI_{100}	UI_{200}	UI_{500}
Cape Frio	OSTIA	DJF	39369	2.15	147	0.023	1.70	2.81	3.88	4.66
Cape Frio	OSTIA	MAM	30963	2.50	164	0.023	1.57	2.72	4.15	5.34
Cape Frio	OSTIA	JJA	18338	2.18	176	0.019	1.12	2.11	3.30	4.52
Cape Frio	OSTIA	SON	20591	1.57	136	0.018	1.14	2.13	2.90	3.38
Cape Frio	OSPO	DJF	38060	2.07	147	0.022	1.55	2.57	3.59	4.41
Cape Frio	OSPO	MAM	32027	2.45	164	0.023	1.48	2.58	3.98	5.13
Cape Frio	OSPO	JJA	18969	2.10	181	0.018	0.93	1.96	3.05	4.28
Cape Frio	OSPO	SON	21092	1.50	147	0.016	0.90	1.81	2.54	3.09
Walvis Bay	OSTIA	DJF	22931	2.67	242	0.018	1.04	1.78	3.61	5.32
Walvis Bay	OSTIA	MAM	6547	3.42	281	0.022	1.08	2.19	4.38	6.76
Walvis Bay	OSTIA	JJA	1839	2.40	292	0.015	0.72	1.42	2.95	4.72
Walvis Bay	OSTIA	SON	34084	2.23	209	0.015	0.90	1.58	3.00	4.43
Walvis Bay	OSPO	DJF	21235	2.53	248	0.016	0.84	1.53	3.26	4.94
Walvis Bay	OSPO	MAM	6764	3.29	286	0.021	0.91	1.95	4.08	6.37
Walvis Bay	OSPO	JJA	2432	2.18	297	0.013	0.50	1.19	2.57	4.19
Walvis Bay	OSPO	SON	33241	2.10	225	0.014	0.54	1.18	2.61	3.99

UC	Product	Season	n	$\bar{D}_{\mathrm{in}}$	x_b	β_{in}	UI_{50}	UI_{100}	UI_{200}	UI_{500}
Lüderitz	OSTIA	DJF	42358	3.81	164	0.040	1.78	4.23	6.45	7.60
Lüderitz	OSTIA	MAM	38454	3.82	198	0.034	1.51	3.46	6.19	7.63
Lüderitz	OSTIA	JJA	32061	2.69	136	0.032	2.32	3.78	5.08	5.86
Lüderitz	OSTIA	SON	40881	2.77	147	0.032	1.91	3.64	5.03	5.74
Lüderitz	OSPO	DJF	39510	3.61	169	0.037	1.12	3.53	5.86	6.86
Lüderitz	OSPO	MAM	38507	3.69	203	0.033	1.13	3.12	5.81	7.19
Lüderitz	OSPO	JJA	32961	2.62	141	0.031	1.99	3.47	4.76	5.49
Lüderitz	OSPO	SON	39601	2.67	153	0.030	1.45	3.24	4.63	5.29
Cape Columbine	OSTIA	DJF	16270	3.12	181	0.034	0.56	3.10	5.14	5.46
Cape Columbine	OSTIA	MAM	15694	3.26	197	0.032	0.61	2.57	5.23	5.82
Cape Columbine	OSTIA	JJA	10814	2.09	158	0.025	0.82	2.23	3.62	3.95
Cape Columbine	OSTIA	SON	14490	1.64	142	0.026	0.77	2.41	3.37	3.11
Cape Columbine	OSPO	DJF	15263	2.86	186	0.032	0.46	2.71	4.81	4.94
Cape Columbine	OSPO	MAM	15833	3.11	203	0.030	0.51	2.31	4.98	5.53
Cape Columbine	OSPO	JJA	11497	1.99	159	0.024	0.72	2.12	3.47	3.77
Cape Columbine	OSPO	SON	14205	1.52	147	0.024	0.64	2.22	3.12	2.80
Cape Peninsula	OSTIA	DJF	16884	2.95	114	0.056	1.56	5.14	5.73	5.29
Cape Peninsula	OSTIA	MAM	15577	3.08	114	0.055	1.98	5.22	6.13	5.86
Cape Peninsula	OSTIA	JJA	5293	1.44	114	0.027	1.57	2.84	3.38	3.17
Cape Peninsula	OSTIA	SON	9466	1.53	108	0.037	1.83	3.82	3.99	3.31
Cape Peninsula	OSPO	DJF	16765	2.68	119	0.052	1.36	4.78	5.32	4.69
Cape Peninsula	OSPO	MAM	16982	2.95	119	0.051	1.71	4.87	5.79	5.50
Cape Peninsula	OSPO	JJA	6425	1.36	114	0.027	1.45	2.69	3.17	2.96
Cape Peninsula	OSPO	SON	10471	1.40	109	0.035	1.57	3.49	3.68	2.91

Table S8: AR(1)-corrected Pearson correlations between the daily $\bar{D}_{\mathrm{in}}$ and the fixed-distance contrast $UI_{\mathrm{SST}}^{(d_0)}$ at $d_0 = 50, 100, 200, 500$ km. Annual rows use all valid daily medians; seasonal rows include the Benjamini–Hochberg adjusted q value for the 40 seasonal r_{50} tests across five UCs, two fine products, and four seasons, reported at the levels $q < 0.05$, $q < 0.01$, $q < 0.001$, and $q < 0.0001$, with n.s. for $q \geq 0.05$.

UC	Product	Period	Season	n	r_{50}	q_{50}	r_{100}	r_{200}	r_{500}
Cape Frio	OSTIA	annual	ANN	3696	+0.24	–	+0.54	+0.78	+0.94
Cape Frio	OSTIA	season	DJF	984	+0.16	< 0.0001	+0.54	+0.76	+0.94
Cape Frio	OSTIA	season	MAM	950	+0.22	< 0.0001	+0.61	+0.83	+0.95
Cape Frio	OSTIA	season	JJA	892	+0.31	< 0.0001	+0.51	+0.75	+0.91
Cape Frio	OSTIA	season	SON	870	+0.08	< 0.05	+0.49	+0.62	+0.88
Cape Frio	OSPO	annual	ANN	3589	+0.34	–	+0.59	+0.82	+0.97
Cape Frio	OSPO	season	DJF	921	+0.41	< 0.0001	+0.70	+0.86	+0.97
Cape Frio	OSPO	season	MAM	951	+0.17	< 0.0001	+0.58	+0.82	+0.98
Cape Frio	OSPO	season	JJA	855	+0.25	< 0.0001	+0.47	+0.78	+0.95
Cape Frio	OSPO	season	SON	862	+0.03	n.s.	+0.39	+0.60	+0.96
Walvis Bay	OSTIA	annual	ANN	2229	+0.28	–	+0.59	+0.77	+0.94
Walvis Bay	OSTIA	season	DJF	782	+0.44	< 0.0001	+0.71	+0.82	+0.94
Walvis Bay	OSTIA	season	MAM	375	+0.00	n.s.	+0.33	+0.56	+0.86
Walvis Bay	OSTIA	season	JJA	167	+0.24	< 0.01	+0.50	+0.73	+0.93
Walvis Bay	OSTIA	season	SON	905	+0.16	< 0.0001	+0.46	+0.66	+0.84
Walvis Bay	OSPO	annual	ANN	2156	+0.40	–	+0.64	+0.80	+0.96
Walvis Bay	OSPO	season	DJF	714	+0.54	< 0.0001	+0.72	+0.82	+0.95
Walvis Bay	OSPO	season	MAM	379	+0.35	< 0.0001	+0.64	+0.75	+0.94
Walvis Bay	OSPO	season	JJA	174	+0.16	n.s.	+0.53	+0.73	+0.95
Walvis Bay	OSPO	season	SON	889	-0.13	< 0.001	+0.31	+0.66	+0.86
Lüderitz	OSTIA	annual	ANN	3972	-0.16	–	+0.27	+0.74	+0.93
Lüderitz	OSTIA	season	DJF	993	-0.02	n.s.	+0.32	+0.69	+0.90
Lüderitz	OSTIA	season	MAM	997	-0.04	n.s.	+0.19	+0.59	+0.86
Lüderitz	OSTIA	season	JJA	988	+0.22	< 0.0001	+0.44	+0.57	+0.84
Lüderitz	OSTIA	season	SON	994	+0.02	n.s.	+0.51	+0.72	+0.86
Lüderitz	OSPO	annual	ANN	3853	-0.25	–	+0.16	+0.71	+0.93
Lüderitz	OSPO	season	DJF	927	-0.02	n.s.	+0.25	+0.66	+0.93
Lüderitz	OSPO	season	MAM	995	-0.16	< 0.0001	+0.03	+0.50	+0.86
Lüderitz	OSPO	season	JJA	972	+0.16	< 0.0001	+0.46	+0.60	+0.89
Lüderitz	OSPO	season	SON	959	+0.03	n.s.	+0.45	+0.67	+0.86
Cape Columbine	OSTIA	annual	ANN	3853	-0.09	–	+0.31	+0.81	+0.95
Cape Columbine	OSTIA	season	DJF	993	+0.01	n.s.	+0.33	+0.68	+0.90
Cape Columbine	OSTIA	season	MAM	1005	+0.06	n.s.	+0.29	+0.68	+0.90
Cape Columbine	OSTIA	season	JJA	888	-0.08	< 0.05	+0.40	+0.76	+0.92
Cape Columbine	OSTIA	season	SON	967	+0.10	< 0.01	+0.54	+0.81	+0.93
Cape Columbine	OSPO	annual	ANN	3765	-0.07	–	+0.25	+0.83	+0.96
Cape Columbine	OSPO	season	DJF	927	+0.10	< 0.01	+0.34	+0.73	+0.93
Cape Columbine	OSPO	season	MAM	999	+0.11	< 0.001	+0.27	+0.72	+0.92
Cape Columbine	OSPO	season	JJA	903	-0.10	< 0.01	+0.36	+0.77	+0.94
Cape Columbine	OSPO	season	SON	936	+0.09	< 0.05	+0.49	+0.80	+0.96
Cape Peninsula	OSTIA	annual	ANN	3335	-0.04	–	+0.72	+0.82	+0.93
Cape Peninsula	OSTIA	season	DJF	982	-0.05	n.s.	+0.60	+0.71	+0.89
Cape Peninsula	OSTIA	season	MAM	978	-0.19	< 0.0001	+0.48	+0.67	+0.87
Cape Peninsula	OSTIA	season	JJA	594	+0.14	< 0.01	+0.48	+0.59	+0.90
Cape Peninsula	OSTIA	season	SON	781	+0.19	< 0.0001	+0.70	+0.78	+0.93
Cape Peninsula	OSPO	annual	ANN	3359	-0.06	–	+0.75	+0.87	+0.96
Cape Peninsula	OSPO	season	DJF	918	+0.02	n.s.	+0.65	+0.79	+0.94
Cape Peninsula	OSPO	season	MAM	978	-0.22	< 0.0001	+0.48	+0.72	+0.91
Cape Peninsula	OSPO	season	JJA	669	+0.20	< 0.0001	+0.54	+0.68	+0.94
Cape Peninsula	OSPO	season	SON	794	+0.06	n.s.	+0.65	+0.78	+0.96

Table S9: AR(1)-corrected alongshore block-bootstrap percentile intervals for the main statistics. The L_r50_ar1 statistic is the Lüderitz OSTIA annual r_{50}; the sBUS statistic is the fine-product southern Benguela SST-structure-only fraction.

Statistic	Block (km)	Replicates	$p_{2.5}$	Median	$p_{97.5}$
L_r50_ar1	25	1000	-0.21	-0.16	+0.04
sBUS_sst_only_ar1	25	1000	+0.17	+0.20	+0.22
L_r50_ar1	50	1000	-0.21	-0.16	+0.13
sBUS_sst_only_ar1	50	1000	+0.16	+0.21	+0.22

Table S10: AR(1)-corrected annual SST-structure phenology summary on OSTIA and OSPO. $\mathrm{NUD_{BR}}$ is the number of SST-structure-active days; $\mathrm{NUE_{BR}}$ is the number of events after bridging one interior inactive day; $\mathrm{TCU_{BR}}$ is the annual sum of daily-median $\bar{D}_{\mathrm{in}}$ over SST-structure-active days.

UC	Product	Years	NUD range	NUD med.	NUE range	NUE med.	TCU range	TCU med.
Cape Frio	OSTIA	11	182–280	221	6–14	11	407–591	507
Cape Frio	OSPO	11	173–285	228	6–12	9	372–584	466
Walvis Bay	OSTIA	11	62–183	118	4–14	8	138–520	310
Walvis Bay	OSPO	11	53–172	117	4–13	6	110–469	254
Lüderitz	OSTIA	11	307–365	339	1–6	3	1034–1191	1147
Lüderitz	OSPO	11	295–363	330	1–5	3	879–1153	1059
Cape Columbine	OSTIA	11	280–364	332	1–9	6	734–983	872
Cape Columbine	OSPO	11	272–362	322	1–9	4	625–922	783
Cape Peninsula	OSTIA	11	200–282	228	3–16	7	472–786	631
Cape Peninsula	OSPO	11	201–288	247	3–10	6	496–743	614

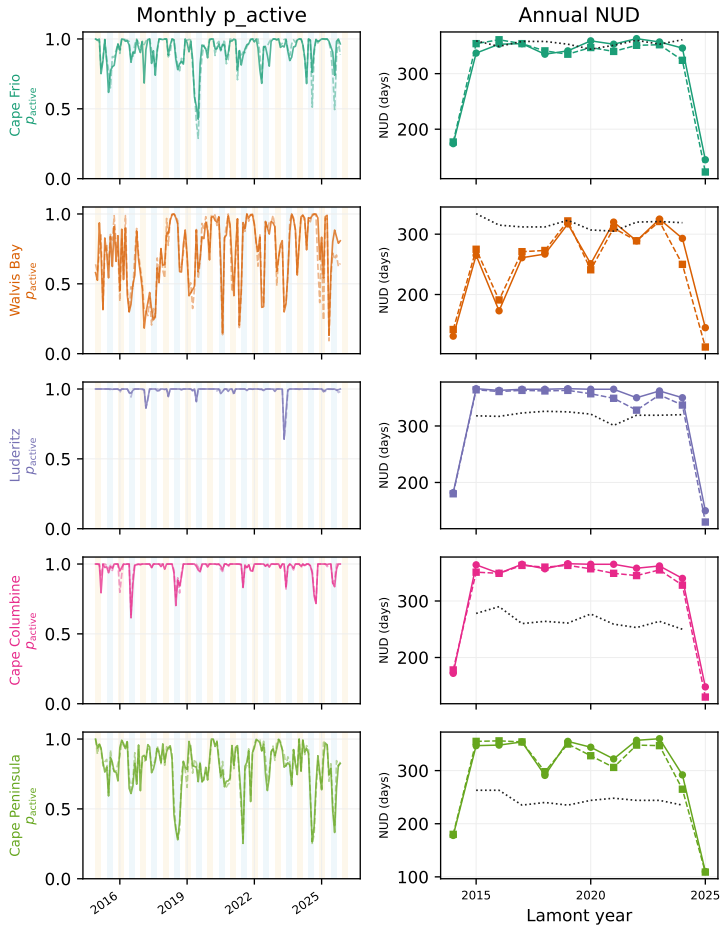

Figure S1. Daily detection and annual upwelling-day phenology within the five Benguela UCs across 2015–2025. Rows are UCs. Left column: monthly aggregate of daily $p_{\mathrm{active}}(c,t)$, the UC-window fraction of accepted breakpoints, as a continuous time series. Right column: per-(UC, year) annual $\mathrm{NUD}_{\mathrm{BR}}$ from the SST-structure detector across the SST products, with the wind-based NUD from Lamont et al. (2018) overlaid as a dotted black line.

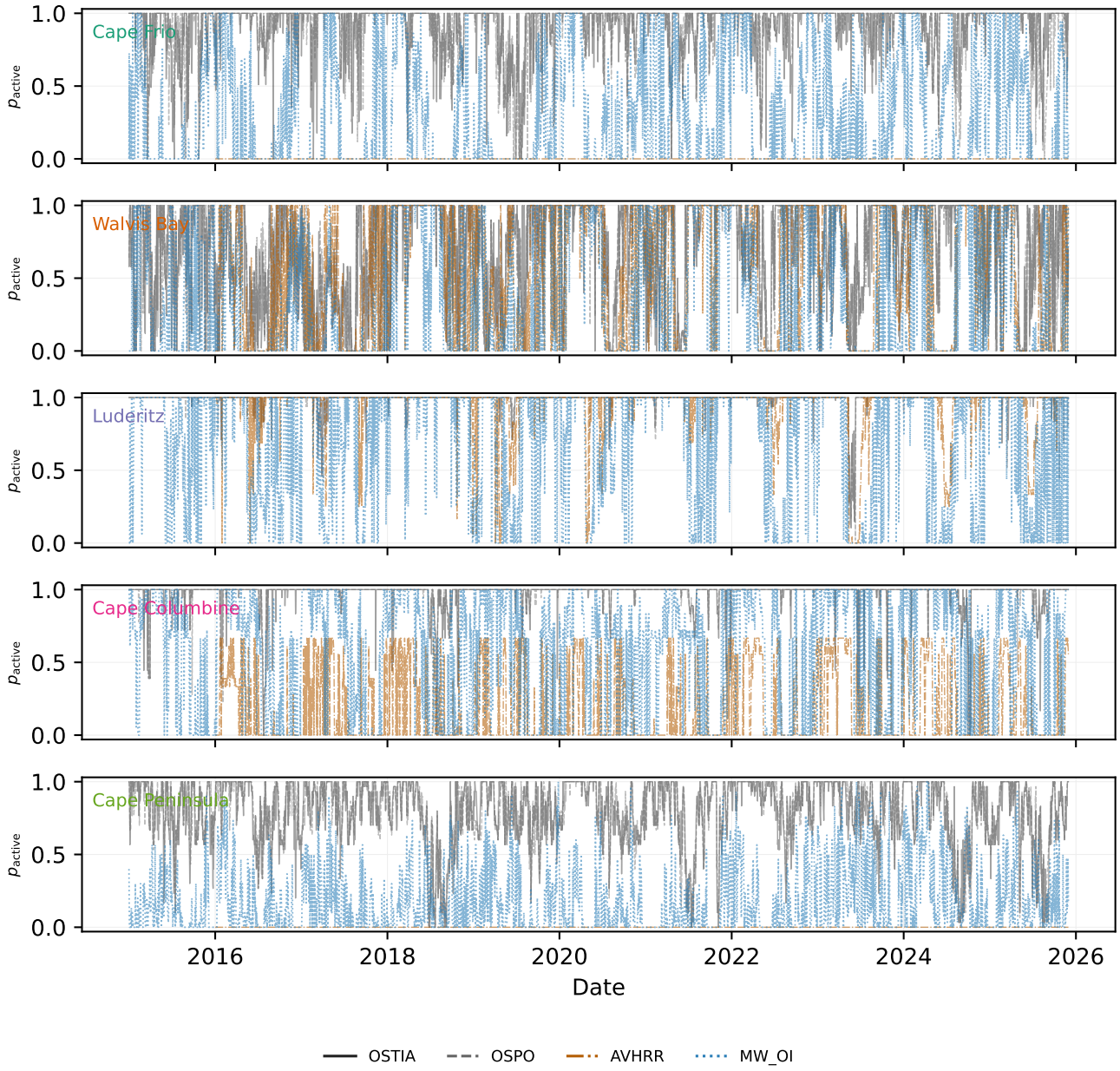

Figure S2. Per-UC daily p_{active} time series across the four SST products, 2015–2025. Each panel is one Benguela UC, and line styles distinguish OSTIA, OSPO, AVHRR, and MW_OI. The figure shows the product-specific daily detection signal before annual phenology aggregation.

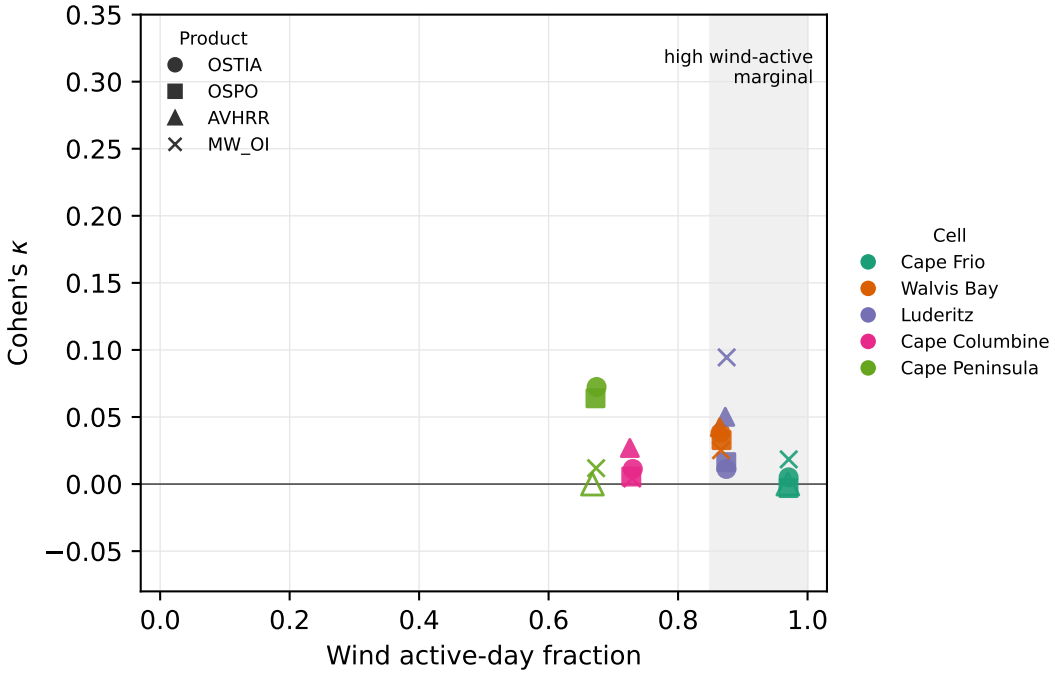

Figure S3. Cohen's κ for the SST–wind daily classifier against the wind active-day marginal probability, by UC and product. Marker shape denotes product and colour denotes UC. The shaded region marks high wind-active marginals, where κ is expected to be compressed because one classifier is active on most days. Open larger markers indicate coverage-artefact product-UC pairs.

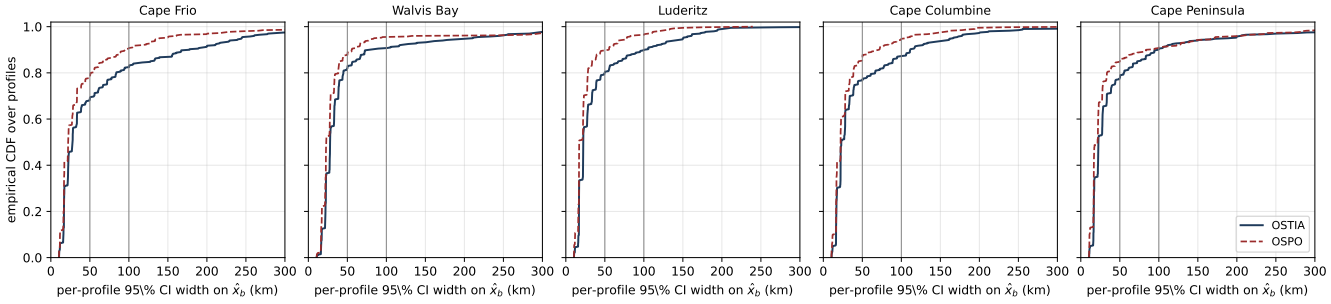

Figure S4. Per-UC empirical cumulative distribution of the per-profile 95 % bootstrap CI width on $\hat{x}_b$, computed on a stratified random sample of 4000 accepted 2020 profiles (100 per (UC, product, season) on OSTIA and OSPO, pooled across the four austral seasons). Each per-profile CI is the 5th–95th percentile spread of 1000 nonparametric bootstrap resamples of the unique-pixel $(x, T_p(x))$ sample with the candidate-grid breakpoint search rerun at each resample. Solid lines are OSTIA, dashed lines are OSPO. Vertical grey lines mark the 50 and 100 km reference widths. The median per-profile CI is 17–28 km across the ten (UC, product) strata, and OSPO carries systematically tighter intervals than OSTIA on the same UC–season combinations. Per-(UC, product) median CI widths, IQR, fractions under 50 and 100 km, and bimodal-flag rates are tabulated in Table S6.

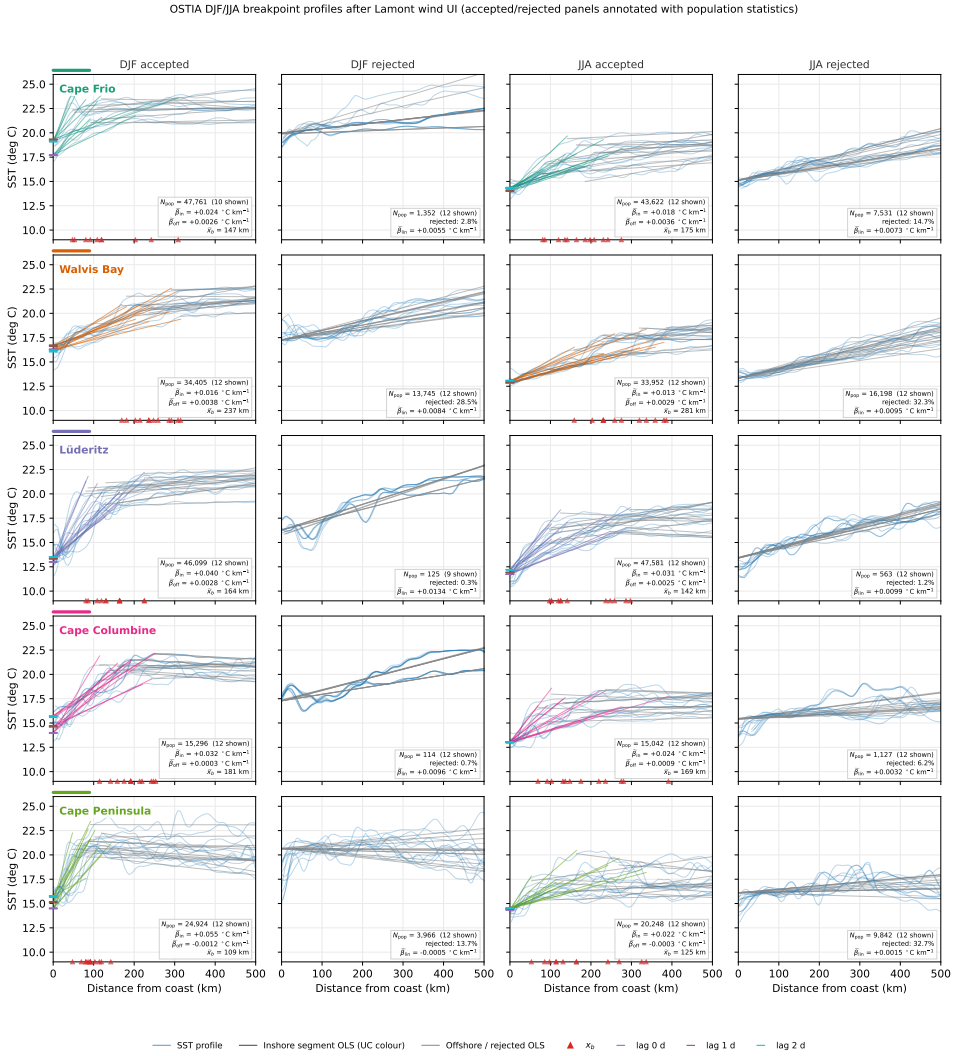

Figure S5. Full-size representative accepted and rejected breakpoint-regression profiles at the five Benguela UCs, OSTIA, 2015–2025, stratified by season. Rows are UCs from Cape Frio to Cape Peninsula; columns are DJF accepted, DJF rejected, JJA accepted, and JJA rejected. In accepted panels the inshore OLS segment is coloured by UC and the offshore OLS segment is grey; in rejected panels the full-profile single-segment OLS fit is the same grey. Annotation boxes report population-level statistics for the full OSTIA panel population, not for the plotted sample.